Synthesis and Characterization of Adducts between SF_4 and Oxygen-Bases: Examples of O---S(IV) Chalcogen Bonding

Dedicated to Karl O. Christe on the occasion of his 80th birthday

James T. Goettel and Michael Gerken*

Contribution from the Canadian Centre for Research in Advanced Fluorine Technologies, University of Lethbridge, Lethbridge, Alberta T1K 3M4, Canada; Department of Chemistry and Biochemistry, University of Lethbridge, Lethbridge, Alberta T1K 3M4, Canada.

* Corresponding author. Tel.: +1-403-329-2173; fax: +1-403-329-2057. *e-mail address*: michael.gerken@uleth.ca.

Abstract

Lewis acid-base adducts between SF_4 and the oxygen-bases THF, cyclopentanone and 1,2-dimethoxyethane were synthesized and characterized by Raman spectroscopy and X-ray crystallography. Crystal structures of $(SF_4{\cdot}OC_4H_8)_2$, $SF_4{\cdot}(OC_4H_8)_2$, $SF_4{\cdot}CH_3OC_2H_4OCH_3$, and $SF_4{\cdot}(O{=}C_5H_8)_2$ show weak S---O chalcogen bonding interactions ranging from 2.662(2) to 2.8692(9) Å. Caffeine, which has three Lewis basic sites, was reacted with SF_4 and one aliquot of HF forming $C_8H_{10}N_4O_2{\cdot}2SF_4{\cdot}HF$ which was also characterized by X-ray crystallography. DFT calculations aided in the assignment of the vibrational spectra of $(SF_4{\cdot}OC_4H_8)_2$, $SF_4{\cdot}(OC_4H_8)_2$, $SF_4{\cdot}CH_3OC_2H_4OCH_3$, and $SF_4{\cdot}(O{=}C_5H_8)_2$. Bonding was studied by Natural Bond Order (NBO) and the Quantum Theory of Atoms in Molecules (QTAIM) analyses.

Introduction

Secondary bonding interactions play an important role in organizing molecules in the condensed phase. One type of secondary bonding interactions is chalcogen bonding, where a σ-hole on a chalcogen atom is acting as an acceptor of electron density from a donor atom, which is frequently a chalcogen atom itself.[1] These interactions are analogous to the more widely known halogen bonding,[2] where a halogen atom acts as an acceptor atom. Generally, chalcogen bonding is stronger for heavier chalcogen atoms with chalcogen bonding to sulfur being on the weaker side. Nevertheless, analysis of crystallographic data has indicated that S---O chalcogen bonding interactions may play a role in biochemical structures, such as protein folding.[3]

Most chalcogen bonding studies involving sulfur as the acceptor atom have focussed on divalent sulfur. Scheiner *et al.* have investigated chalcogen bonding for tetravalent sulfur by computational means.[4,5] The molecular electrostatic potential (MEP) of SF_4 shows two σ-holes,[4] which explains the experimentally observed coordination of two fluoride ions to SF_4,[6] as well as the weak interactions between fluorine and sulfur in the crystal structure of SF_4.[7] Interestingly, the MEP maxima, *i.e.*, the σ-holes, for SF_4 have a similar value compared to those of divalent H_2S (SF_4: 176.6 kJ/mol; H_2S: 176.4 kJ/mol).[4]

In our investigations of the Lewis-acid behaviour of SF_4, we conclusively showed the formation of 1:1 Lewis acid-base adducts with a number of nitrogen bases, *i.e.*, pyridine,[8] 4-methylpyridine,[8] 2,6-dimethylpyridine,[8] 4-dimethylaminopyridine,[8] and triethylamine.[9] The S---N chalcogen bonds in these adducts are weak and the adducts dissociate above −35 °C under dynamic vacuum. Sulfur tetrafluoride has been shown to combine with uncoordinated, 'naked' fluoride to form the SF_5^- anion.[10] The crystal structures of $Rb^+[SF_5^-]$,[11] $Cs^+{}_6[SF_5^-]_4[HF_2^-]_2$,[11] $[Cs(18\text{-crown-}6)_2^+][SF_5^-]$,[12] $[HNC_5H_3(CH_3)_2^+]_2F^-[SF_5^-]\cdot 4SF_4$,[7] $[HNC_5H_3(CH_3)_2^+]_2F^-[SF_5^-]\cdot SF_4$,[6]

and $[HNC_5H_4N(CH_3)_2^+]_2[SF_5^-]F^-\cdot CH_2Cl_2$[6] confirmed the square pyramidal geometry of the SF_5^- anion that is predicted by the VSEPR rules. In cases where the fluoride is not 'naked', dramatically weaker interactions between SF_4 and F^- are observed in the solid state.[6] In contrast to the 1:1 adducts with nitrogen bases, sulfur in SF_4 accepts two coordinative bonds from two F^- anions.

Since SF_4 has been used as a deoxofluorinating reagent in organic chemistry,[13] the interaction between SF_4 with oxygen-bases is of particular interest in order to elucidate the mechanism of deoxofluorination reactions. Based on the ^{19}F chemical shift of SF_4 in THF (OC_4H_8) and ethyl acetate, Muetterties suggested that SF_4 does not form adducts with these two oxygen bases.[14] Azeem, on the other hand, concluded from changes in $\delta(^{19}F)$ and the decrease in $^2J(^{19}F–^{19}F)$ coupling of SF_4 in THF and diethylether solvents that $SF_4\cdot OC_4H_8$ and $SF_4\cdot O(C_2H_5)_2$ adducts form at low temperatures.[15] Two new bands (680 and 1706 cm^{-1}) in the infrared spectrum of matrix-isolated SF_4 with acetone in an N_2 matrix were also interpreted in terms of the formation of a 1:1 adduct.[16] More recently, a computational study has investigated intramolecular S---O interactions in substituted phenyl-SF_3 molecules.[17] Because of the lack of conclusive experimental information about Lewis acid-base interactions between SF_4 and O-bases, the goal of the current study was to investigate whether S---O chalcogen bonding interactions are sufficiently strong to isolate adducts between SF_4 and organic oxygen-bases, such as a cyclic ether (tetrahydrofuran), an open-chain diether (dimethoxyethane), and a ketone (cyclopentanone).

The heaviest chalcogen analogue of SF_4, TeF_4, which is significantly more Lewis acidic than SF_4, reacts with various cyclic and acyclic ethers to form the adducts $TeF_4\cdot$1,4-dioxane,[18] $TeF_4\cdot$(1,2-dimethoxyethane)$_2$,[18] $TeF_4\cdot Et_2O$,[18] and $TeF_4\cdot(THF)_2$,[19] which have been structurally characterized by X-ray crystallography. The related $SeF_2(CN)_2$ has recently been found to form adducts with O-bases, such as 1:2 adduct with THF, $SeF_2(CN)_2\cdot(THF)_2$.[20]

Results and Discussion

Synthesis and Properties

The reactions of SF_4 with representative oxygen-bases were studied by low-temperature Raman spectroscopy and X-ray crystallography. Mixtures of SF_4 and THF in various ratios form clear colourless liquids between −60 to −90 °C, which have lower vapour pressures than neat SF_4 or THF. A 1:1 mixture of SF_4 and THF freezes at −99 °C, forming a clear colourless crystalline solid whereas a 1:2 mixture of SF_4 to THF freezes at a lower temperature (−106 °C). As shown by Raman spectroscopy and X-ray crystallography, two distinct adducts were obtained from the two reactant ratios (Eq. 1).

$$SF_4 + nOC_4H_8 \rightleftharpoons SF_4{\cdot}(OC_4H_8)_n \quad (\text{where } n = 1, 2) \qquad (1)$$

Cyclopentanone is miscible with an equimolar amount of SF_4 at −50 °C. The mixture solidifies at approximately −100 °C; however, the solid melts at −63 °C (Eq. 2). X-ray crystallography showed a 1:2 molar ratio of SF_4 vs. cyclopentanone. The nature of the solid was also confirmed by Raman spectroscopy.

$$SF_4 + 2\ O{=}C_5H_8 \rightleftharpoons SF_4{\cdot}(O{=}C_5H_8)_2 \qquad (2)$$

A mixture of 1,2-dimethoxyethane in excess SF_4 was placed under dynamic vacuum at −90 °C for several hours. Mass balance measurements indicated that the mixture obtained after the removal of excess SF_4 corresponded to an approximate 1:1 molar ratio of SF_4 to 1,2-dimethoxyethane. The product froze at −105 °C to form a clear colourless crystalline solid which was identified by Raman spectroscopy and X-ray crystallography as the $SF_4{\cdot}CH_3OC_2HOCH_3$ adduct. (Eq. 3) It remains solid at −83 °C, but with vigorous agitation will revert back to the liquid state.

$$SF_4 + CH_3OH_2H_4OCH_3 \rightleftharpoons SF_4{\cdot}CH_3OC_2H_4OCH_3 \qquad (3)$$

The SF_4·O-base adducts dissociate when warmed above −60 °C or placed under reduced pressure. Unlike the nitrogen-base adducts, mixtures of SF_4 with oxygen-bases do not appear to be sensitive to the presence of traces of HF and no solvolysis products analogous to those previously reported were observed.[6]

In order to ascertain interactions of SF_4 with a molecular system that has several Lewis basic sites caffeine was chosen, having two carbonyl groups and one N-basic site. Since caffeine does not dissolve appreciably in SF_4 and no reaction at room temperature was observed, one aliquot of HF was added, resulting in good solubility. Hydrogen fluoride was generated by addition of H_2O that hydrolyzed excess SF_4 to HF and SOF_2, as reported in our previous study.[6] It had been found that the hydrolysis product SOF_2 does not interfere with the chemistry in these systems. Crystals were grown from liquid SF_4 and found to have the composition $C_8H_{10}N_4O_2$·2SF_4·HF (Eq. 4).

$$2SF_4 + C_8H_{10}N_4O_2 + HF \rightarrow C_8H_{10}N_4O_2{\cdot}2SF_4{\cdot}HF \qquad (4)$$

X-ray Crystallography

Details of data collection parameters and crystallographic information for $(SF_4{\cdot}OC_4H_8)_2$, $SF_4{\cdot}(OC_4H_8)_2$, $SF_4{\cdot}CH_3OC_2H_4OCH_3$, $SF_4{\cdot}(O{=}C_5H_8)_2$ and $C_8H_{10}N_4O_2{\cdot}2SF_4{\cdot}HF$ are given in Table S1. Selected bond lengths and angles are listed in Table 1 together with the predicted values based on DFT calculations and the experimental, as well as predicted geometries are depicted in Figure 1. Full lists of metric parameters are given in Tables S2 to S6.

Table 1 Selected Bond Lengths (Å), Contacts (Å), and Angles (°) of $(SF_4{\cdot}OC_4H_8)_2$, $SF_4{\cdot}(OC_4H_8)_2$, $SF_4{\cdot}(O{=}C_5H_8)_2$, $SF_4{\cdot}CH_3OC_2H_4OCH_3$, and $C_8H_{10}N_4O_2{\cdot}2SF_4{\cdot}HF$.

$(SF_4{\cdot}OC_4H_8)_2$					
Bond Lengths and Contacts, Å			Bond Angles, deg.		
	Expt.	Calcd.		Expt.	Calcd.
S–F_{eq}	1.534(2) to 1.547(2)	1.584, 1.585	F_{eq}–S–F_{eq}	98.3(1), 98.5(1)	98.581, 98.55
S–F_{ax}	1.643(2) to 1.661(2)	1.700 to 1.704	F_{ax}–S–F_{ax}	173.8(1), 171.6(1)	172.13, 172.14
S---O	2.777(2) to 2.802(2)	2.895, 2.902	O---S---O	102.12(6), 102.03(5)	98.05, 98.08
			S---O---S	77.49(5), 77.97(4)	81.86, 82.01
			F_{eq}–S---O	175.99(8) to 178.47(8)	177.84, 177.84
$SF_4{\cdot}(OC_4H_8)_2$					
Bond Lengths and Contacts, Å			Bond Angles, deg.		
	Expt.	Calcd.[a]		Expt.	Calcd.[a]
S–F_{eq}	1.528(2) to 1.546(2)	1.581, 1.589	F_{eq}–S–F_{eq}	96.5(1) to 97.1(1)	97.52
S–F_{ax}	1.626(2) to 1.658(2)	1.705, 1.713	F_{ax}–S–F_{ax}	171.1(1) to 172.6(1)	172.43
S---O	2.662(2) to 2.792(2)	2.739, 2.872	O---S---O	107.25(7) to 112.86(7)	102.77
			F_{eq}–S---O	168.69(10) to 174.42(9)	176.64, 174.12
$SF_4{\cdot}(O{=}C_5H_8)_2$					
Bond Lengths and Contacts, Å			Bond Angles, deg.		
	Expt.	Calcd.[a]		Expt.	Calcd.[a]
S–F_{eq}	1.546(1), 1.548(1)	1.588, 1.576	F_{eq}–S–F_{eq}	98.24(6)	98.42
S–F_{ax}	1.658(1), 1.667(1)	1.712, 1.703	F_{ax}–S–F_{ax}	171.85(6)	172.19
S---O	2.759(1), 2.788(1)	2.966, 2.797	O---S---O	105.46(4)	96.64
C=O	1.215(2), 1.216(2)	1.211,1.210	F_{eq}–S---O	173.57(5), 177.00(5)	170.94, 175.23
$SF_4{\cdot}CH_3OC_2H_4OCH_3$					
Bond Lengths and Contacts, Å			Bond Angles, deg.		
	Expt.	Calcd.[a,b]		Expt.	Calcd.[a,b]
S–F_{eq}	1.5474(7)	1.574	F_{eq}–S–F_{eq}	99.03(5)	98.88
S–F_{ax}	1.660(1), 1.674(1)	1.705, 1.712	F_{ax}–S–F_{ax}	171.41(5)	173.07
S---O	2.8692(9)	2.996	O---S---O	107.49(4)	100.99
			F_{eq}–S---O	168.37(3)	172.79, 172.50
$C_8H_{10}N_4O_2{\cdot}2SF_4{\cdot}HF$					
Bond Lengths and Contacts, Å			Bond Angles, deg.		
	Expt.			Expt.	
S_1–F_{eq}	1.5354(13), 1.5440(13)		F_{eq}–S_1–F_{eq}	99.74(8)	
S_1–F_{ax}	1.6462(14), 1.6717(14)		F_{ax}–S_1–F_{ax}	172.50(7)	
S_1---O	2.8586(17), 2.9954(18)		O---S_1---O	103.78(5)	
S_2–F_{eq}	1.5466(12), 1.5483(13)		F_{eq}–S_2–F_{eq}	99.30(7)	
S_2–F_{ax}	1.6556(14), 1.6706(13)		F_{ax}–S_2–F_{ax}	171.48(6)	
S_2---O	2.8034(19)		O---S_2---F	96.94(5)	
S_2---F	2.7932(15)		F_{eq}–S_1---O	179.51(6)	
			F_{eq}–S_1---F	175.44(5)	

	F_{eq}–S_2---O	173.13(6),174.26(6)

[a] Calculated at the B3LYP/aug-cc-pVTZ level of theory [b] Predicted for the DMESF_4DME adduct.

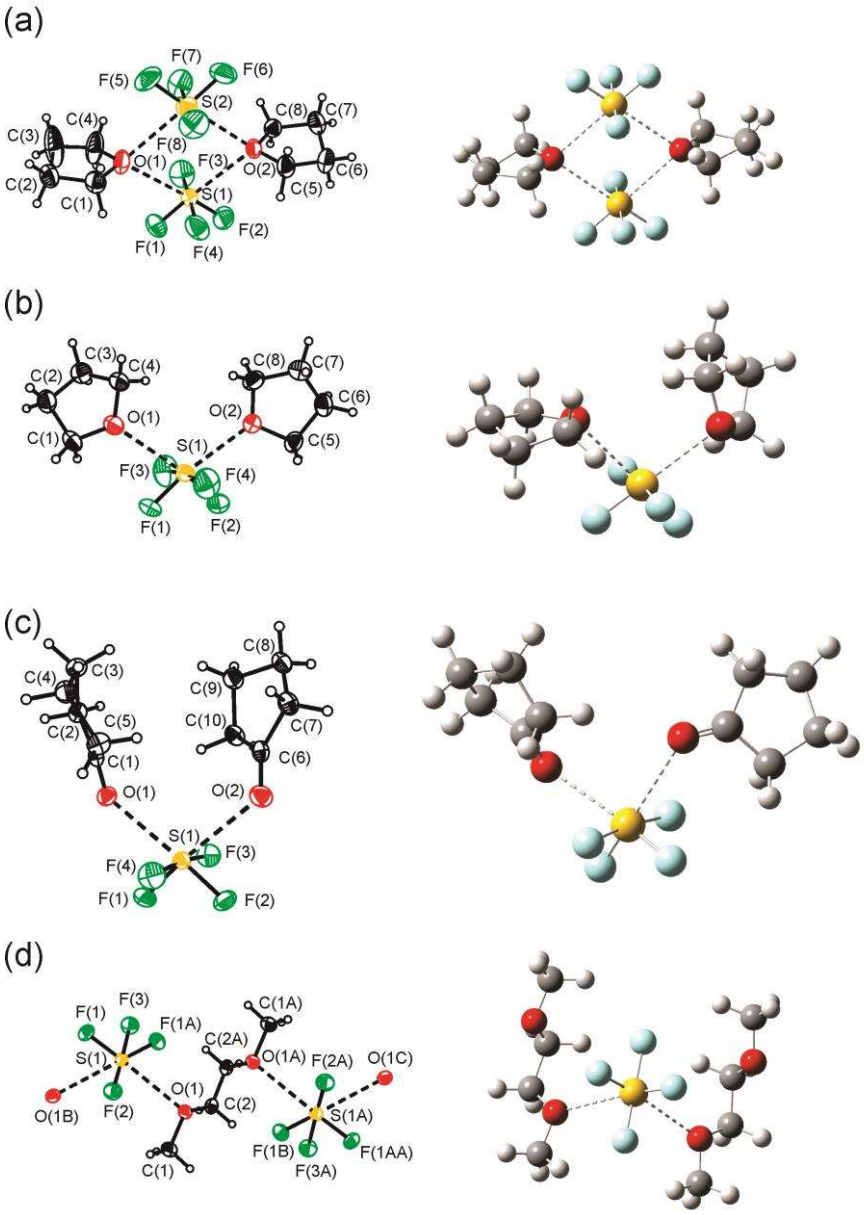

Figure 1 Thermal ellipsoid plots of (a) the $(SF_4 \cdot OC_4H_8)_2$ dimer, (b) one of the four crystallographically independent $SF_4 \cdot (OC_4H_8)_2$, (c) the $SF_4 \cdot (O{=}C_5H_8)_2$ molecule, and (d) part of the chain of the $SF_4 \cdot CH_3OC_2H_4OCH_3$ structure. Thermal ellipsoids are set at 50% probability. Optimized gas-phase geometries are shown of $(SF_4 \cdot OC_4H_8)_2$, $SF_4 \cdot (OC_4H_8)_2$, $SF_4 \cdot (O{=}C_5H_8)_2$, and $SF_4 \cdot (CH_3OC_2H_4OCH_3)_2$ on the right side.

The 1:1 adduct between SF_4 and OC_4H_8 crystallizes in the monoclinic space group $P2_1/n$, with two SF_4 and two THF molecules in the asymmetric unit. The structure consists of $(SF_4 \cdot OC_4H_8)_2$ dimers that contain two SF_4 molecules bridged by the oxygen atoms of two THF molecules (Figure 1a). The coordination of SF_4 by two oxygens of THF in the $(SF_4 \cdot OC_4H_8)_2$ dimer prompted the preparation and investigation of the 1:2 adduct $SF_4 \cdot (OC_4H_8)_2$ which crystallizes in the triclinic space group $\boldsymbol{P\bar{1}}$. The asymmetric unit of $SF_4 \cdot (OC_4H_8)_2$ contains four independent, well separated adduct molecules (Figures 1b and S1). As expected from the coordination environment of sulfur in $(SF_4 \cdot OC_4H_8)_2$, two THF molecules coordinate to one sulfur atom of each SF_4 molecule. In an analogous fashion, two cyclopentanone molecules coordinate to one SF_4 in the 1:2 adduct $SF_4 \cdot (O{=}C_5H_8)_2$ (Figure 1c), which crystallizes in the monoclinic space group $P2_1/n$. Based on the coordination of two Lewis basic oxygens towards sulfur in $(SF_4 \cdot OC_4H_8)_2$, $SF_4 \cdot (OC_4H_8)_2$, and $SF_4 \cdot (O{=}C_5H_8)_2$, the possibility of forming a chelate complex with a bidentate ligand was explored. The bidentate ligand, 1,2-dimethoxyethane, which had been shown to form a chelate complex with TeF_4,[18] was used to form adducts with SF_4. The resulting adduct, $SF_4 \cdot CH_3OC_2H_4OCH_3$, crystallizes in the orthorhombic space group *Pbcm*. Instead of acting as a chelating ligand, 1,2-dimethoxyethane bridges two SF_4 molecules, resulting in a chain structure (Figure 1d).

In all adducts with the O-bases, the coordination number about sulfur is extended to six, with two S---O chalcogen bonds. The two S---O distances are the same for $SF_4 \cdot CH_3OC_2H_4OCH_3$ or somewhat different for the other adducts (difference of 0.025 Å, $(SF_4 \cdot OC_4H_8)_2$; 0.130 Å, $SF_4 \cdot (OC_4H_8)_2$; 0.029 Å, $SF_4 \cdot (O{=}C_5H_8)_2$). This coordination mode is in stark contrast to the geometry of SF_4·N-base adducts, in which only one nitrogen atom coordinates towards SF_4 resulting in a square-pyramidal geometry about sulfur.[8,9] In the SF_4·O-base adducts the seesaw geometry of free SF_4 is retained upon coordination of two O-bases with S---O bond lengths ranging

between 2.662(2) and 2.8692(9) Å, which are smaller than the sum of the van der Waals radii (3.32 Å), but substantially longer than the S---N distances in the crystal structures of SF_4·N-base adducts (2.141(2) to 2.514(2) Å).[8,9] The longer S---O chalcogen bonds are a consequence of the lower Lewis basicity of the O-bases compared to the N-bases and the fact that two base molecules compete for the Lewis acidity of the same sulfur center. The O-bases avoid the lone pair on sulfur, resulting in O---S---O angles between 105.49(4) and 117.86(7)° for $SF_4·(OC_4H_8)_2$ and $SF_4·CH_3OC_2H_4OCH_3$, respectively. The O---S---O angles in $(SF_4·OC_4H_8)_2$ are significantly smaller (102.12(6) and 102.03(5)°) because of constraints from the formation of the four-membered S_2O_2 ring in the dimer. This geometric constraint in the $(SF_4·OC_4H_8)_2$ dimer also results in small S---O---S angles of 77.49(5) and 77.97(4)°. For all adducts, the oxygen atoms are essentially in the same plane as the sulfur atom and the equatorial fluorine atoms of SF_4. As a consequence, the F_{eq}–S–F_{eq} angles in the adducts are contracted to values ranging from 96.5(1) to 99.03(5)° compared to those in free SF_4 ($SF_{4(g)}$: 101.6(5)/103.8(6)°,[21,22] $SF_{4(s)}$: 99.6(3)/101.0(2)°).[7] The F_{eq}–S–F_{eq} angle is the largest for the adduct with 1,2-dimethoxyethane (99.03(5)°), which exhibits the longest S---O distances, whereas it is the smallest for the 1:2 adduct with THF (96.5(1) to 97.1(1)°), which has the shortest S---O distances among the studied O-base adducts. The contraction of the F_{eq}–S–F_{eq} angle in SF_4 is, however, not as dramatic as in the adducts between SF_4 and a nitrogen base (89.98(11) to 95.74(9)°).[8] The F_{ax}–S–F_{ax} angle does not change appreciably upon adduct formation between SF_4 and O-bases when compared to solid and gaseous SF_4 ($SF_{4(g)}$: 173.1(5)°,[21] $SF_{4(s)}$: 171.6(3)/172.6(3)°).[7] Such an almost negligible effect on F_{ax}–S–F_{ax} angle had also been observed for the SF_4·N-base adducts with the smallest F_{ax}–S–F_{ax} angle (169.70(14)°) for the SF_4·4-$NC_5H_4N(CH_3)_2$ adduct, which exhibits the strongest S---N interaction.[8] The equatorial S–F bond lengths in the O-base adducts range from 1.528(2) to 1.5478(10) Å,

which are, as expected, significantly shorter than the axial bond lengths that range from 1.626(2) to 1.6736(10) Å. The experimental S−F bond lengths in the adducts are not significantly different from those of solid SF_4 (S−F_{eq}: 1.474(6) to 1.553(4) Å; S−F_{ax}: 1.635(4) to 1.676(5) Å), reflecting the weakness of the Lewis acid base interactions.

In the $(SF_4{\cdot}OC_4H_8)_2$ dimer, the thermal ellipsoids of the carbons (C(4), C(5) Figure 1 a.) on one of the two THF molecule are elongated, reflecting a high degree of thermal motion, *i.e.*, puckering of the THF ring, which is a common occurrence with THF. The small size of the carbon thermal ellipsoids in $SF_4{\cdot}(O{=}C_5H_8)_2$ indicates less thermal motion in the carbon ring of cyclopentanone. The C=O lengths of the cyclopentanone molecules in the SF_4 adduct (1.215(2) and 1.216(2) Å) are in the range of bond lengths found for neat cyclopentanone (1.2109(15) and 1.2148(15) Å)) reflecting the insignificant effect of SF_4 coordination on the geometry of cyclopentanone.[23] The 1,2-dimethoxyethane molecule lies on a crystallographic C_2-axis and adopts the gauche conformation that has previously been predicted to be the stable conformation for free 1,2-dimethoxyethane.[24]

To the best of our knowledge, these structures represent the first examples of oxygen-bases coordinating to a S(IV) center as well as the $(SF_4{\cdot}OC_4H_8)_2$ dimer represents a rare structure in which an organic oxygen-base is coordinated to two non-metals. A search of the Cambridge Crystal Database for coordination complexes of a neutral organic oxygen-base to sulfur gave only one result where dioxane is coordinated to SO_3.[25]

In general, the geometry of the SF_4O_2 moiety in the adducts is well reproduced by the geometry optimization at the B3LYP/DFT level of theory. The predicted conformations of the THF and cyclopentanone rings in the gas-phase structures of the mononuclear adducts, however, are different from those found in the crystal structure. The differences can be explained by subtle

intramolecular interactions in the gas phase, such as very weak CH···FS hydrogen-bonding interactions, which are easily overruled by solid-state effects. Similarly, the conformation of the dimethoxyethane (DME) ligands in the optimized gas-phase geometry of DME·SF_4·DME is very different to that observed in the solid-state chain structure. The predicted S–F and S---O bond lengths are systematically longer than the experimental ones, but the F–S–F angles are reproduced well. The overestimation of bond lengths was previously observed in the study of SF_4 nitrogen base adducts.[8] Whereas the slight asymmetry in the experimental S---O distances is well reproduced for the THF adducts, the difference in the two predicted S---O distances for SF_4·$(O{=}C_5H_8)_2$ (0.17 Å) is substantially larger than that observed in the crystal structure (0.03 Å). This discrepancy is likely a consequence of the difference in conformation of the two cyclopentanone ligands. Despite the difference in predicted S---O distances for SF_4·$(O{=}C_5H_8)_2$, the predicted C=O bond lengths of the two $O{=}C_5H_8$ molecules in the adducts are essentially the same. The predicted O---S---O angles for SF_4·$(O{=}C_5H_8)_2$ and SF_4·$(OC_4H_8)_2$ are significantly smaller than the crystallographically observed values, reflecting the facile deformability of this angle. For the $(SF_4{\cdot}OC_4H_8)_2$ dimer the O---S---O angles are also predicted to be smaller than the observed ones, likely as a consequence of the weaker predicted S---O interaction. This is paralleled by larger predicted S---O---S angles.

Caffeine has three Lewis basic sites, *i.e.*, one nitrogen, N(4) and two C=O groups. The addition of one HF aliquot was expected to solvolyse one base---S interaction, as observed in our previous study.[6] The structure of $C_8H_{10}N_4O_2{\cdot}2SF_4{\cdot}HF$ (Figure 2) contains two independent SF_4 molecules that exhibit C=O---S interactions with both carbonyl groups of caffeine, which were not affected by HF. For one SF_4 molecule, two symmetry-related carbonyl-oxygens, i.e., O(2) and O(2A), bridge two symmetry-related SF_4 molecules, forming a four-membered S_2O_2 ring,

structurally similar to that in $(SF_4 \cdot OC_4H_8)_2$. The second SF_4 molecule forms one C=O---S contact to the other carbonyl oxygen, i.e., O(1), and an F---S contact to the fluorine atom of HF, which is hydrogen bonded to the Lewis basic N(4) atom of caffeine. The S---O distances in this structure are significantly longer than those in $SF_4 \cdot (O=C_5H_8)_2$. In light of the present work with oxygen-bases and our previous work about F_4S---F interactions, this hexacoordination is not unexpected.

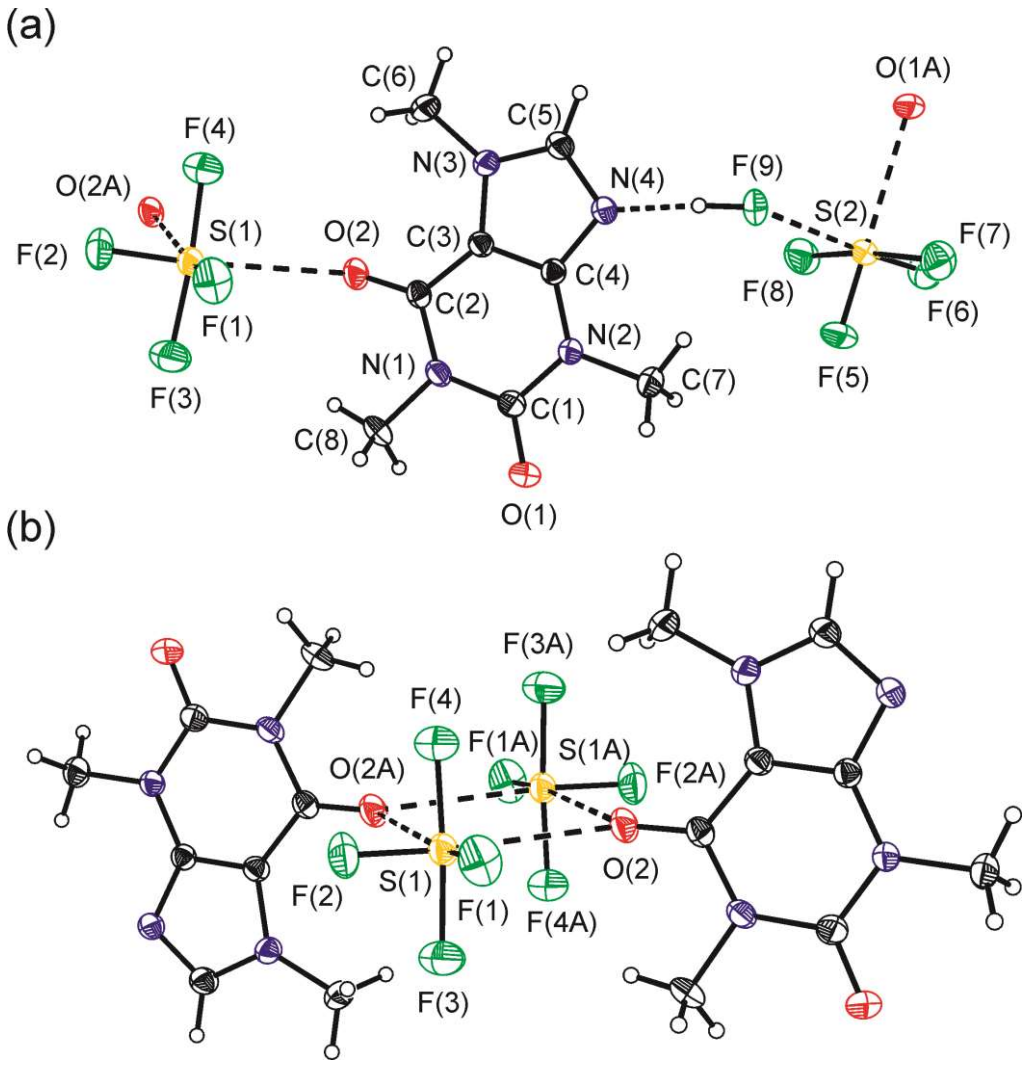

Figure 2 Thermal ellipsoid plot of (a) the asymmetric units and contacts in $C_8H_{10}N_4O_2 \cdot 2SF_4 \cdot HF$ and (b) the coordination mode about $S(1)F_4$. Thermal ellipsoids are set at 50% probability.

The geometry about sulfur in these adducts could be classified as AX_4Y_2E VSEPR-type. For main-group elements with seven electron groups the pentagonal bipyramid is generally

preferred, as observed for main-group fluorides such as IF_7 (AX_7 VSEPR geometry),[26] IOF_5^{2-} (AX_5YE VSEPR geometry),[27] and XeF_5^- (AX_5E_2 VSEPR geometry).[28] In contrast, for the AX_6E geometry with a stereochemically active lone pair, a distorted octahedral geometry has been found.[29] For the SF_4·O-base adducts, two fluorine atoms are in the axial positions, while two fluorine atoms, two oxygen atoms, and the lone pair are located in the equatorial plane. The F_{eq}–S–F_{eq} (96.5(1) to 99.03(5)°) and F_{eq}–S–O (75.69(3) to 79.72(8)°) angles are significantly larger than the ideal angles for a pentagonal plane (72°). Instead of considering the S---O interactions as full bonding electron-pair domains, they need to be viewed as weak secondary bonding interactions, *i.e.*, chalcogen bonds, that do not fundamentally change the geometry of the SF_4 molecule. Chalcogen bonding interactions had been found to have a directionality as a consequence of the location of the σ-holes. For SF_4, two σ-holes were predicted on the molecular electrostatic potential of sulfur.[5] These σ-holes were located opposite of the equatorial S–F bonds, suggesting a preference for an approximate linear F_{eq}–S---O arrangement, which is experimentally supported by the observation of F_{eq}–S---O angles ranging from 168.7(1) to 178.47(8)°.

Comparing SF_4 with its tellurium analogue, the larger Lewis acidity of TeF_4 is apparent. As in the 1:2 adducts of SF_4 with THF, $TeF_4 \cdot 2OC_4H_8$ consists of monomeric units with two Te---O chalcogen bonds. These two Te---O bonds are quite short (2.448(2) and 2.697(2) Å), reflecting the larger Lewis acidity of TeF_4 compared to SF_4.[19] In contrast to the coordination chemistry towards SF_4, the 1,2-dimethoxyethane acts as a chelating ligand towards the chalcogen centre in TeF_4.[18] It is interesting to note that TeF_4 even forms an adduct with two 1,2-dimethoxyethane ligands coordinated to Te in a bidentate fashion. The resulting coordination number of 8 about Te is possible because of the much larger atomic radius of tellurium versus that of sulfur. A chelating

coordination of 1,2-dimethoxyethane towards SF_4 is apparently geometrically disfavoured because of the small size of sulfur.

Raman Spectroscopy

Solid $(SF_4 \cdot OC_4H_8)_2$, $SF_4 \cdot (OC_4H_8)_2$, $SF_4 \cdot CH_3OC_2H_4OCH_3$, and $SF_4 \cdot (O{=}C_5H_8)_2$ were characterized by Raman spectroscopy at −110 °C and the spectra are depicted in Figures 3 to 5 together with those of the free bases. Experimental, as well as predicted vibrational frequencies of the SF_4O_2 moiety of the adducts are listed in Table 2, together with the approximate mode descriptions. Complete lists of experimental and predicted vibrational frequencies are provided in the Supporting Information (Tables S7 to S10). The assignments of the vibrational bands are based on the computational results and comparison with the vibrational frequencies of the free bases and SF_4. The assignment and description of the modes associated with THF, cylcopentanone and 1,2-dimethoxyethane are also based on the spectroscopic and computational work by Berthier *et al.*,[30] Cataliotti and Paliani,[31] and Yoshida and Matsuura.[32]

Table 2. Observed and Calculated Frequencies and Their Assignments for the O_2SF_4 Moieties in the $(SF_4{\cdot}OC_4H_8)_2$, $SF_4{\cdot}(OC_4H_8)_2$, $SF_4{\cdot}(O{=}C_5H_8)_2$, and $SF_4{\cdot}CH_3OC_2H_4OCH_3$ Adducts

SF_4		$(SF_4{\cdot}OC_4H_8)_2$		$SF_4{\cdot}(OC_4H_8)_2$		$SF_4{\cdot}(O{=}C_5H_8)_2$		$SF_4{\cdot}CH_3OC_2H_4OCH_3$		assignments[d]
exptl[a]	calcd[a,b]	exptl[c]	calcd[b]	exptl[c]	calcd[b]	exptl[c]	calcd[b]	exptl[c]	calcd[b]	
892	856(13)[104]	859(100) 848(12)	823(144)[45] 820(1)[316]	847(100) 826(41)	823(93)[175]	872(88)	836(83)[176]	850(100)	848(34)[23]	$\nu_s(SF_{2,\ eq})$
867	825(4)[170]	774(6)	797(0)[512] 788(38)[0]	773(2)	787(27)[280]	831(21)	794(46)[243]	773(1)	819(9)[224]	$\nu_{as}(SF_{2,eq})$
730	703(<1)[630]	621(4)	676(0)[793] 643(1)[0]	634(3) 579(5)	649(1)[467]	639(5)	652(1)[558]	610(4) 579(5)	645(1)[473]	$\nu_{as}(SF_{2,ax})$
558	535(12)[3]	527(84)	515(13)[0] 512(0)[5]	518(91)	506(8)[1]	532(41) 526(47) 519(36)	508(10)[3]	522(12) 512(40)	508(7)[1]	$\nu_s(SF_{2,\ ax})$
532	500(<1)[<1]	n.o.	485(0)[4] 483(0)[8]	n.o.	479(<1)[11]	n.o.	481(1)[14]	n.o.	482(<1)[12]	$\rho_w(SF_{2,eq})$
532	494(3)[19]	n.o.	486(1)[3] 482(0)[45]	n.o.	484(1)[26]	n.o.	485(1)[29]	n.o.	487(2)[24]	$\delta_{sc}(SF_{2,\ eq}) + \delta_{sc}(SF_{2,\ ax})$
475	436(1)[<0.1]	446(8)	421(1)[0] 419(1)[0]	445(7)	415(1)[0]	401(2)	419(1)[0]	453(7)	419(1)[0]	$\tau(SF_2)$
353	327(<0.1)[10]	381(10)	333(0)[24] 329(0)[1]	381(9)	335(0)[18]	n.o.	332(<1)[13]	n.o.	325(0)[24]	$\delta_{sc,\ out\text{-}of\text{-}plane}(SF_{2,\ ax})$
228	211(<1)[1]	256(6)	235(0)[8] 231(2)[0]	266(6)	240(2)[1]	260(5)	233(2)[1]	255(3)	236(0)[0]	$\delta_{sc}(SF_{2,\ eq}) - \delta_{sc}(SF_{2,\ ax})$
		n.o. n.o.	112(0)[1] 66(1)[0]	n.o.	69(1)[0]	n.o.	78(1)[3]	n.o.	70(0)[0]	$\nu_s(SO_2)$
		n.o. n.o.	49(0)[0] 43(1)[0]	n.o.	61(1)[1]	n.o.	66(1)[1]	n.o.	65(<1)[2]	$\nu_{as}(SO_2)$

[a] Experimental gas-phase vibrational frequencies and assignments from ref. 33. The calculated frequencies are essentially the same as in ref. 33 but no scaling factors were used for the listed frequencies. [b] Calculated at the B3LYP/aug-cc-pVTZ level of theory. Unscaled Raman intensities, in $Å^4\ u^{-1}$, are given in parentheses; infrared intensities, in km mol^{-1}, are given in square brackets. [c] The abbreviations denote not observed (n.o.) and shoulder (sh). Complete lists of Raman frequencies are given in the Supporting Information (Tables S1 to S4). Values in parentheses denote relative intensities. [d] The abbreviations denote symmetric (s), antisymmetric (as), stretch (ν), bend (δ), twist (τ), wagging (ρ_w), and rock (ρ_{rock}). The numbering scheme refers to that used in Figure 1.

The Raman spectra of the four adducts contain bands attributable to vibrations of the O-base and SF_4 moieties with only a few modes predicted to exhibit vibrational coupling of SF_4 and the base. The S–F stretching bands of all four adducts are shifted to lower frequencies compared to those of free SF_4,[33] reflecting an increase in ionic character of S–F bonding in adducts. The Raman band associated with the $\nu_s(SF_{2eq})$ mode in neat SF_4 (896 cm^{-1}) is significantly lowered upon adduct formation to 859 ($(SF_4 \cdot OC_4H_8)_2$), 847 cm^{-1} ($SF_4 \cdot (OC_4H_8)_2$), 872 cm^{-1} ($SF_4 \cdot (O{=}C_5H_8)_2$), and 850 cm^{-1} ($SF_4 \cdot CH_3OC_2H_4OCH_3$). Similarly, the $\nu_s(SF_{2ax})$ band of neat SF_4 (558 cm^{-1}) is significantly shifted to lower frequencies in the adducts ($(SF_4 \cdot OC_4H_8)_2$), 527 cm^{-1}; ($SF_4 \cdot (OC_4H_8)_2$), 518 cm^{-1}; ($SF_4 \cdot (O{=}C_5H_8)_2$), 519 cm^{-1}; $SF_4 \cdot CH_3OC_2H_4OCH_3$, 522/512 cm^{-1}).

Most Raman bands attributable to the O-base moieties exhibit shifts relative to those of the free O-base. The complexation shifts of THF for $(SF_4 \cdot OC_4H_8)_2$ and $SF_4 \cdot (OC_4H_8)_2$ are the same or very similar. For example, the most intense band in the Raman spectrum of neat THF (ν_s(C–C), 914 cm^{-1}) is shifted to 923 cm^{-1} in the spectra both adducts. The CO stretching bands of cyclopentanone (1743/1728 cm^{-1}) are shifted to 1724/1712 cm^{-1} for $SF_4 \cdot (O{=}C_5H_8)_2$, reflecting the weakening of the CO bond upon formation of the adduct. In general, the observed complexation shifts for the three O-bases are significantly larger than the predicted shifts, which can be explained by the underestimation of the predicted Lewis acid-base interactions.

Whereas vibrational coupling of the two THF moieties in $SF_4 \cdot (OC_4H_8)_2$ is predicted to result in splitting of a few bands with a maximum splitting of 14 cm^{-1}, none of those predicted splittings were resolved. The two THF moieties in dimeric $(SF_4 \cdot OC_4H_8)_2$ are predicted to exhibit stronger vibrational coupling because of the more rigid cyclic structure. As a result, three bands in the experimental Raman spectrum exhibit splittings. In the Raman spectrum of $SF_4 \cdot (O{=}C_5H_8)_2$, a number of bands are split. For the 1,2-dimethoxyethane adduct, the vibrational coupling was

predicted to be negligible, which is paralleled with no resolved splitting in the experimental spectrum.

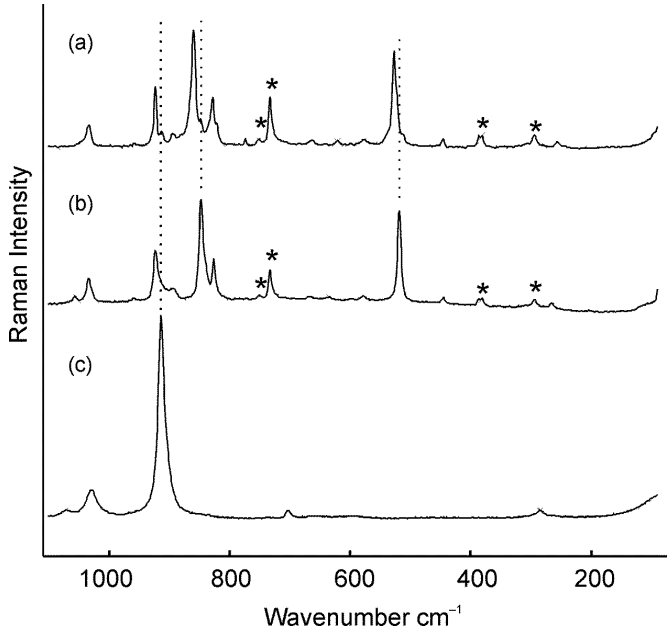

Figure 3 Raman spectra of a) $(SF_4 \cdot OC_4H_8)_2$ (at −110 °C), b) $SF_4 \cdot (OC_4H_8)_2$ (at −107 °C), and c) OC_4H_8 (room temperature). Asterisks (*) denote bands arising from the FEP sample tube.

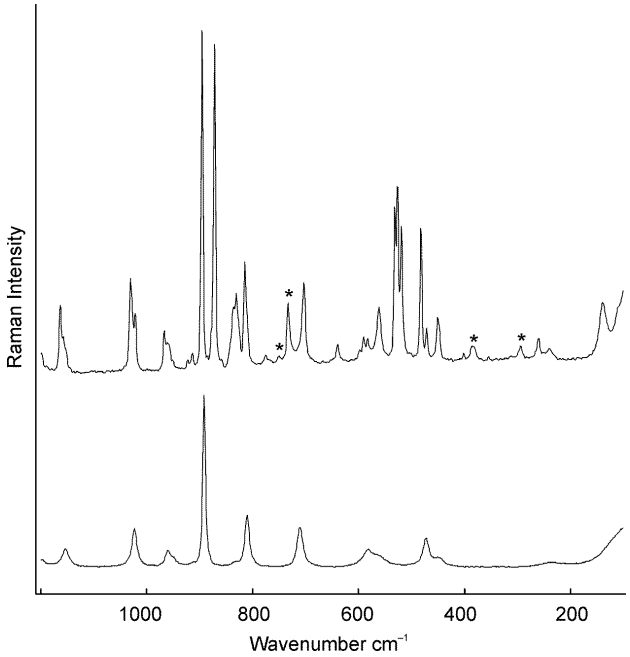

Figure 4 Raman spectra of $SF_4 \cdot (O{=}C_5H_8)_2$ at −110 °C (upper trace) and neat cyclopentanone ($O{=}C_5H_8$) at room temperature (lower trace). Asterisks (*) denote bands arising from the FEP sample tube.

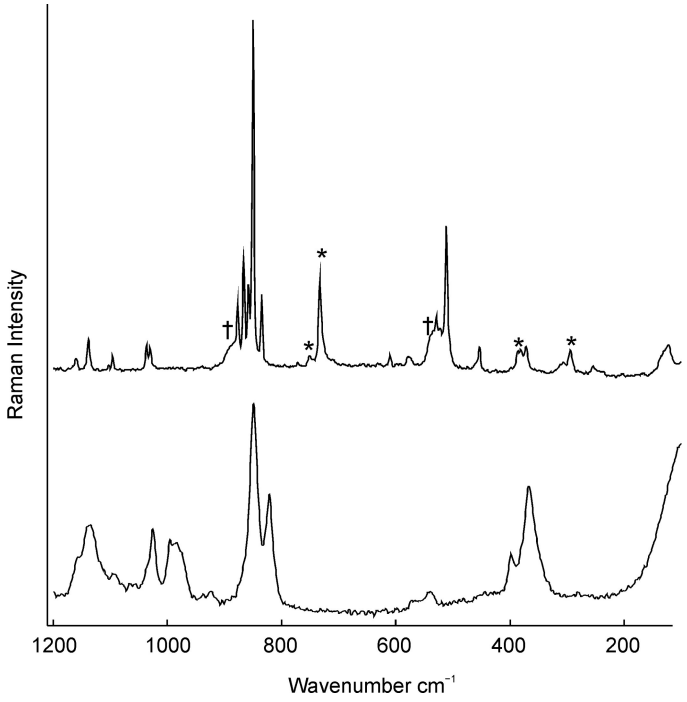

Figure 5 Raman Spectrum of $SF_4 \cdot CH_3OC_2H_4OCH_3$ at −110 °C (upper trace) and neat 1,2-dimethoxyethane at room temperature (lower trace). Asterisks (*) and daggers (†) denote bands arising from the FEP sample tube and residual SF_4, respectively.

Computational Results.

The electronic structures of $(SF_4 \cdot OC_4H_8)_2$, $SF_4 \cdot (OC_4H_8)_2$, and $SF_4 \cdot (O{=}C_5H_8)_2$, as well as those of the free oxygen-bases, were optimized in the gas phase using the B3LYP/aug-cc-pVTZ method, where each structure is a stationary point at the potential energy surface and all frequencies are real. To reproduce the vibrational frequencies of the 1,2-dimethoxyethane adduct, the geometries of the $SF_4 \cdot (CH_3OC_2H_4OCH_3)_2$ and $(CH_3OC_2H_4OCH_3) \cdot SF_4 \cdot (CH_3OC_2H_4OCH_3)$ adducts were optimized and vibrational frequencies were calculated. The optimized geometries of $(SF_4 \cdot OC_4H_8)_2$, $SF_4 \cdot (OC_4H_8)_2$, $SF_4 \cdot (O{=}C_5H_8)_2$, and $SF_4 \cdot (CH_3OC_2H_4OCH_3)_2$ adducts are depicted in Figure 1 and selected calculated metric parameters are listed in Table 2. A complete list of calculated metric parameters is provided in the Supporting Information. Natural bond order (NBO) analyses and quantum theory of atoms in molecules (QTAIM) were carried out (Tables S14 to S21).

While the experimental geometries about sulfur for $(SF_4 \cdot OC_4H_8)_2$, $SF_4 \cdot (OC_4H_8)_2$, and $SF_4 \cdot (O{=}C_5H_8)_2$ were reproduced well by the calculations, the predicted conformations of the ligands in these adducts exhibit significant differences compared to the experimental structures. Those differences can be attributed to F---H hydrogen bonding interactions in the gas-phase structures, which manifest themselves in bond paths obtained from the QTAIM analyses. The associated bond critical points have extremely small electron densities ($\rho_b \leq 0.006$ a.u.), which is a sign of the weakness of these hydrogen bonds. In the case of dimeric $(SF_4 \cdot OC_4H_8)_2$, a S---S bond path was also observed. Those weak interactions resulted in a number of ring critical points and, for $SF_4 \cdot (O{=}C_5H_8)_2$ and $SF_4 \cdot (CH_3OC_2H_4OCH_3)_2$, cage critical points.

The electron density at the bond critical point, ρ_b, of the S---O chalcogen bonds for the SF_4·O-base adducts are very small ($SF_4 \cdot (OC_4H_8)_2$: 0.021 and 0.016 a.u.; $SF_4 \cdot (O{=}C_5H_8)_2$: 0.019 and 0.013 a.u.; $SF_4 \cdot (CH_3OC_2H_4OCH_3)_2$: 0.012 and 0.011 a.u.). These ρ_b values are significantly lower than those found for the SF_4·N-base ($SF_4 \cdot NC_5H_5$: 0.037 a.u.),[8] illustrating the weakness of the S---O chalcogen bonding interactions. The small ρ_b values are accompanied by significant positive values of the Laplacian of the electron density at the bond critical point, $\nabla^2\rho_b$ ($SF_4 \cdot (OC_4H_8)_2$: 0.053 and 0.069 a.u.; $SF_4 \cdot (O{=}C_5H_8)_2$: 0.044 and 0.060 a.u.; $SF_4 \cdot (CH_3OC_2H_4OCH_3)_2$: 0.041 a.u.), which is characteristic for closed-shell, electrostatic interactions, such as chalcogen-bonding interactions of the oxygen lone pairs with the σ-holes on sulfur. These values are within those found for hydrogen-bonds, which have ρ_b values between 0.002 to 0.035 a.u. and $\nabla^2\rho_b$ values of 0.024 to 0.139 a.u.[34] The charge transfer from the ligand to SF_4 can be calculated as the sum of the atomic basin charges for SF_4 moiety in the adducts ($SF_4 \cdot OC_4H_8)_2$: −0.055/−0.051; $SF_4 \cdot (OC_4H_8)_2$: −0.071; $SF_4 \cdot (O{=}C_5H_8)_2$: −0.056; $SF_4 \cdot (CH_3OC_2H_4OCH_3)_2$: −0.039). As expected, the transferred charge is

substantially smaller than that in SF_4·N-base adducts, such as $SF_4{\cdot}NC_5H_5$ (−0.115),[8] in spite of the donation of electron density from two oxygens.

Adduct formation results in an increase of the NPA charges on sulfur and fluorine, indicating an increase of ionic character. As a consequence, the equatorial and axial S−F bond orders are somewhat smaller in the adducts compared to those in free SF_4. The bond orders for the S---O bonds are smaller by one order of magnitude than those of the S−F bonds. NBO second order perturbation analysis showed that the donation of electron density from the lone pairs of oxygen, O_{lp1} and O_{lp2}, into the σ*(S−F) orbital trans to the S---O contacts provides stabilization. The stabilization energies, E(2), for $SF_4{\cdot}(OC_4H_8)_2$ and $SF_4{\cdot}(O{=}C_5H_8)_2$ are 20.75 kJ/mol (from O(1): 12.97 kJ/mol; from O(2): 7.78 kJ/mol) and 15.07 kJ/mol (from O(1): 10.88 kJ/mol; from O(2): 4.19 kJ/mol) per sulfur atom, respectively. As expected, the NBO E(2) energies for dimeric $(SF_4{\cdot}OC_4H_8)_2$ are smaller with 13.1 kJ/mol for each sulfur atom, because each oxygen donates electron density to two sulfur centres. The NBO E(2) value per sulfur atom for $SF_4{\cdot}(CH_3OC_2H_4OCH_3)_2$ is significantly smaller with 5.90 kJ/mol. Calculations of the enthalpies of adduct formation for the molecular 1:2 adduct, $SF_4{\cdot}(OC_4H_8)_2$ and $SF_4{\cdot}(O{=}C_5H_8)_2$, from SF_4 and the O-bases in the gas phase revealed negative enthalpy values of −12.27 and −13.15 kJ/mol, respectively. As expected from the weakness of the chalcogen bonding interactions, the exothermicity of these reactions is lower than those for the formation of the SF_4·N-base adducts $SF_4{\cdot}N(C_2H_5)_3$ (−15.98 kJ/mol), $SF_4{\cdot}NC_5H_5$ (−23.12 kJ/mol), $SF_4{\cdot}NC_5H_4CH_3$ (−24.84 kJ/mol), and $SF_4{\cdot}NC_5H_4N(CH_3)_2$ (−30.99 kJ/mol). The addition of the first O-base molecule to SF_4 contributes the most of the exothermicity (Table S22), however, a detailed analysis of the enthalpies of the two steps should be considered with caution because of the effect of weak intra (F---HC hydrogen bonding) and intermolecular interactions on the small enthalpy of reaction values.

Summary and Conclusion

For the first time, experimental proof for chalcogen bonding of oxygen-bases to SF_4 is presented by the isolation and structural characterization of SF_4·O-base adducts. Adduct formation was observed with the three oxygen-bases THF, 1,2-dimethoxyethane, and cyclopentanone at low temperatures. It was crucial to handle these adducts at temperatures below −60 °C to avoid dissociation because of the weakness of their Lewis-acid-base interaction. The isolation of the first SF_4·ketone adduct SF_4·$(O{=}C_5H_4)_2$ is of particular interest, since SF_4 can serve as a fluorinating agent towards carbonyl groups. In the solid-state structures of the adducts, sulfur accepts chalcogen bonds from two Lewis-basic oxygens, increasing the coordination environment about sulfur to six. The two S---O chalcogen bonds are directed towards the previously predicted σ-holes on sulfur in SF_4.[4] This observation is in contrast to SF_4·N-base adducts in which only one nitrogen base coordinates to SF_4 to form a square pyramidal geometry about sulfur.[8,9] In the SF_4·N-base adducts, one molecule of the more Lewis-basic N-bases donates sufficient electron density towards sulfur, lowering the Lewis acidity of the resulting adduct and circumventing the coordination of the second N-base molecule. In addition, the closer proximity of the N-base may prevent the coordination of a second base molecule. Therefore, both electronic and steric arguments likely contribute in preventing facile coordination of a second nitrogen base.

Quantification of Lewis basicity is difficult, since it depends on the nature of the Lewis acid. The most extensive list of Lewis basicity values is that for the BF_3 affinity scale.[35] Although BF_3 is a harder acid than SF_4, we found in our previous studies that the trends in BF_3 affinity values describe the strength of the organic bases towards SF_4 well.[8] The BF_3 affinity of THF (90 kJ mol^{-1}) is the highest in the series of O-bases of this study, followed by cyclopentanone (77 kJ mol^{-1}) and 1,2-dimethoxyethane (75 kJ mol^{-1}).[35] Those donor strengths, which are significantly smaller than

those of the N-bases DMAP (152 kJ mol^{-1}) and pyridine (128 kJ mol^{-1}),[35] generally follow an inverse relationship with the observed S---O distances ($SF_4 \cdot (OC_4H_8)_2$: average of 2.711 Å; $SF_4 \cdot (O{=}C_5H_8)_2$: average of 2.774 Å; $SF_4 \cdot (CH_3OC_2H_4OCH_3)$: 2.8692(9) Å).

Experimental Section

Caution! *Sulfur tetrafluoride is volatile and corrosive gas which has toxicity similar to that of phosgene. Hydrogen fluoride is also highly toxic and corrosive. Compounds should be disposed of in a concentrated base inside a fume hood. Care should be taken to minimize exposure to SF_4 while mounting crystalline samples.*

Materials and Apparatus. Tetrahydrofuran was handled on a Pyrex vacuum line equipped with glass/Teflon J. Young valves. Sulfur tetrafluoride was handled on a vacuum line constructed of nickel, stainless steel, and tetrafluoroethylene-hexafluoropropylene-copolymer (FEP). Reaction vessels were fabricated from ¼-in. o.d. FEP tubing and outfitted with Kel-F valves. Tetrahydrofuran (Fisher, HPLC grade) was refluxed with benzophenone and sodium, and vacuum distilled onto freshly cut sodium. Dimethoxyethane (Fisher, 99.9%), cyclopentanone (BDH, 99%), and caffeine (Pure Bulk, 99%) were used as received. Sulfur tetrafluoride (Ozark-Mahoning Co.) was purified by passing the gas through an FEP U-trap containing activated charcoal. Traces of thionyl fluoride and sulfur hexafluoride were present in the sulfur tetrafluoride, as observed by ^{19}F NMR spectroscopy, but did not interfere with the chemistry.

Preparation of $(SF_4 \cdot OC_4H_8)_2$. Tetrahydrofuran (0.233 g, 3.23 mmol) was distilled into a ¼-in. FEP reactor. Sulfur tetrafluoride (0.35 g, 3.2 mmol) was transferred into the reactor at −196 °C. The reactor was allowed to warm to −80 °C in an ethanol bath and agitated, forming a clear colorless solution. Slow cooling of the reactor caused the solution to solidify at *ca.* −99 °C. Small

Raman bands at 848(12) and 513sh cm^{-1} in the Raman spectrum of $(SF_4 \cdot OC_4H_8)_2$ indicated an impurity of $SF_4 \cdot (OC_4H_8)_2$.

Preparation of $SF_4 \cdot (OC_4H_8)_2$. Tetrahydrofuran (0.172 g, 2.39 mmol) was distilled into a ¼-in. FEP reactor. Sulfur tetrafluoride (0.13 g, 1.2 mmol) was transferred into the reactor at −196 °C and the reactor was warmed to −80 °C. The solution was mixed forming a clear colorless solution. Slow cooling of the reactor cause the solution to solidify at *ca*. −106 °C.

Preparation of $SF_4 \cdot (CH_3OC_2H_4OCH_3)$. In a fume-hood, 1,2-dimethoxyethane (0.037 g, 0.41 mmol) was transferred into a ¼-in. FEP reactor using a glass pipette. The 1,2-dimethoxyethane was then degassed using the freeze-pump-thaw method. Excess SF_4 (0.231 g, 2.14 mmol) was vacuum distilled into the reactor at −196 °C. The reactor was slowly warmed to −60 °C in order to completely dissolve the solid 1,2-dimethoxyethane forming a clear colorless solution. No precipitate was observed when the reactor was cooled to −110 °C. The reactor was warmed to −90 °C and placed under dynamic vacuum in order to remove excess SF_4 for *ca*. 2 hours, after which the Raman spectrum still showed small broad bands arising from residual SF_4. The reactor was slowly cooled causing the liquid to crystallize at *ca*. −100 °C. The solid (81 mg, 0.41 mmol) melted at ca. −83 °C. Crystals suitable for X-ray diffraction were grown from the melt by slow cooling to −110 °C.

Preparation of $SF_4 \cdot (O{=}C_5H_8)_2$. In a fume-hood, cyclopentanone (20 mg, 0.24 mmol) was transferred into a ¼-in. FEP reactor using a glass pipette. The cyclopentanone was then degassed using the freeze-pump-thaw method. Sulfur tetrafluoride (26 mg, 0.24 mmol) was vacuum distilled onto the frozen cyclopentanone at −196 °C. The reactor was warmed to −50 °C and vigorously agitated in order to completely dissolve the solid cyclopentanone. The reactor was slowly cooled

to −100 °C causing the liquid to crystallize. The colourless crystalline solid melted at approximately −63 °C.

Preparation of $C_8H_{10}N_4O_2 \cdot 2SF_4 \cdot HF$. Caffeine (42 mg, 0.22 mmol) was loaded into a ¼-in. FEP reactor and placed under dynamic vacuum overnight. Using a micro syringe, H_2O (0.002 mg, 0.1 mmol) was added into the reactor. Excess SF_4 (*ca.* 0.3 mL) was distilled into the reactor at −196 °C. The reactor was warmed to the melting point of SF_4 and the reaction was quenched with liquid N_2. The reactor was slowly warmed while mixing to completely dissolve the fine white solid. Slow cooling of the clear colorless solution to −80 °C caused the formation of large crystalline plates.

Raman Spectroscopy. All Raman spectra were recorded on a Bruker RFS 100 FT Raman spectrometer with a quartz beam splitter, a liquid-nitrogen cooled Ge detector, and R-496 temperature accessory. The actual usable Stokes range was 50 to 3500 cm^{-1}. The 1064-nm line of an Nd:YAG laser was used for excitation of the sample. The Raman spectra were recorded with a spectral resolution of 2 cm^{-1} using laser powers of 150 mW.

X-ray Crystallography. Crystals were mounted at low temperature under a stream of dry cold nitrogen as previously described,[36] except sample tubes were cut and manipulated in the cold trough at low temperatures. The crystals were removed with the tip of a glass pipette and were directly affixed onto either a glass fiber, or a nylon cryo-loop dipped in inert perfluorinated polyethers, Fomblin Z-25 or Z-15 (Ausimont Inc.). The use of a round FEP tray, inside the trough, was also used to manipulate crystals which decomposed on contact with the metal troughs. The crystals were centered on a Bruker SMART APEX II diffractometer, controlled by the APEX2 Graphical User Interface software.[37] The program SADABS[38] was used for scaling of diffraction data, the application of a decay correction, and a multi-scan absorption correction. Program SHELXS-2014/6 (Sheldrick, 2014)[39] was used for both solution and refinement. Structure

solutions were obtained by direct methods. CCDC 1507214 to 1507218 contain the crystallographic data. These data can be obtained free of charge from The Cambridge Crystallographic Data Centre via www.ccdc.cam.ac.uk/data_request/cif.

Computational Methods

Quantum-chemical calculations were carried out using the Gaussian 09 program package.[40] Geometries and frequencies were fully optimized using density functional theory (DFT) at the B3LYP/aug-cc-pVTZ level. The natural bond orbital (NBO) analysis was performed using the NBO-6 program.[41] The wavefunctions obtained from the DFT calculations were analysed according to the quantum theory of atoms in molecules (QTAIM) using the AIM11/AIMStudio suite of programs.[42] The GaussView program was used to visualize the vibrational displacements that form the basis for the vibrational mode descriptions.[43]

Acknowledgements

We thank the Natural Sciences and Engineering Research Council of Canada (NSERC), the Canadian Foundation for Innovation (CFI), and the University of Lethbridge for funding.

References

(1) (a) Wang, W.; Ji, B.; Zhang, Y. Chalcogen Bond: A Sister Noncovalent Bond to Halogen Bond. *J. Phys. Chem. A* **2009**, *113*, 8132-8135; (b) Karjalainen, M. M.; Sanchez-Perez, C.; Rautianinen, J. M.; Oilunkaniemi, R.; Laitinen, R. S. Chalcogen–Chalcogen Secondary Bonding Interactions in Trichalcogenaferrocenophanes. *Cryst. Eng. Comm.* **2016**, *18*, 4538-4545.

(2) Cavallo, G.; Metrangolo, P.; Milani, R.; Pilati, T.; Priimagi, A.; Resnati, G.; Terraneo, G. The Halogen Bond. *Chem. Rev.* **2016**, *116*, 2478-2601.

(3) Iwaoka, M.; Takemoto, S.; Tomoda, S. Statistical and Theoretical Investigations on the Directionality of Nonbonded S···O Interactions. Implications for Molecular Design and Protein Engineering. *J. Am. Chem. Soc.* **2002**, *124*, 10613-10620.

(4) Nziko, V.D.P.N.; Scheiner, S. Chalcogen Bonding between Tetravalent SF_4 and Amines. *J. Phys. Chem. A* **2014**, *118*, 10849-10856.

(5) Azofra, L. M.; Alkorta, I.; Scheiner, S. Chalcogen Bonds in Complexes of SOXY (X, Y = F, Cl) with Nitrogen Bases. *J. Phys. Chem. A* **2015**, *119*, 535-541.

(6) Goettel, J. T.; Kostiuk, N.; Gerken, M. Interactions between SF_4 and Fluoride: A Crystallographic Study of Solvolysis Products of SF_4·Nitrogen-Base Adducts by HF. *Inorg. Chem.* **2016**, *55*, 7126-7134.

(7) Goettel, J. T.; Kostiuk, N.; Gerken, M. The Solid-State Structure of SF_4: The Final Piece of the Puzzle. *Angew. Chem. Int. Ed.* **2013**, *52*, 8037-8040.

(8) Chaudhary, P.; Goettel, J. T.; Mercier, H. P. A.; Sowlat-Hashjin, S.; Hazendonk, P.; Gerken, M. Lewis Acid Behavior of SF_4: Synthesis, Characterization, and Computational Study of Adducts of SF_4 with Pyridine and Pyridine Derivatives. *Chem. Eur. J.* **2015**, *21*, 6247-6256.

(9) Goettel, J. T.; Chaudhary, P.; Mercier, H. P. A.; Hazendonk, P.; Gerken, M. SF_4·$N(C_2H_5)_3$: The First Conclusively Characterized SF_4 Adduct with an Organic Base *Chem. Commun.* **2012**, *48*, 9120-9122.

(10) Tunder, R.; Siegel, B. The SF_5 Anion. *J. Inorg. Nucl. Chem.* **1963**, *25*, 1097-1098.

(11) Bittner, J.; Fuchs, J.; Seppelt, K. Die Kristallstruktur des SF_5^--Anions. *Z. Anorg. Allg. Chem.* **1988**, *557*, 182-190.

(12) Clark, M.; Kellen-Yuen, C.; Robinson, K.; Zhang, H.; Yang, Z.-Y.; Madappat, K.; Fuller, J.; Atwood, J.; Thrasher, J. "Naked" SF_5^- anion: The crystal and molecular structure of $[Cs^+.(18\text{-crown-}6)_2][SF_5^-]$ *Eur. J. Solid State Inorg. Chem.* **1992**, *29*, 809-833.

(13) Dmowski, W. Introduction of Fluorine Using Sulfur Tetrafluoride and Analogs, In Organo-Fluorine Compounds, Methods of Organic Chemistry; Baasner, B.; Hagemann, H.; Tatlow, J. C.; Eds.; Houben-Weyl, Vol. E10a, Thieme, Stuttgart, 2000, ch. 8, pp. 321-431.

(14) Muetterties, E. L. Sulfur Tetrafluoride Adducts. U.S. Patent 2,729,663: 1959.

(15) Azeem, M. 1:1 Adducts of SF_4 with Tetrahydrofuran and Diethylether. *Pak. J. Sci. Ind. Res.* **1967**, *10*, 10-12.

(16) Sass, C. S.; Ault, B. S. Matrix Isolation Infrared Spectroscopic Study of the 1:1 Molecular Complexes Between the Sulfur Fluorides and Oxyfluorides and Selected Bases. *J. Phys. Chem.* **1985**, *89*, 1002-1006.

(17) Nziko, V.D.P.N.; Scheiner, S. Intramolecular S···O Chalcogen Bond as Stabilizing Factor in Geometry of Substituted Phenyl-SF_3 Molecules. *J. Org. Chem.* **2015**, *80*, 2356-2363.

(18) Shlykov, S. A.; Giricheva, N. I.; Titov, A. V.; Szwak, M.; Lentz, D.; Girichev, G. V. The Structures of Tellurium (IV) Halides in the Gas Phase and as Solvated Molecules. *Dalton Trans.* **2010**, *39*, 3245-3255.

(19) Lentz, D.; Szwak, M. Synthesis and Structure Determination of Tellurium Tetracyanide Solvates: Pseudopolymorphism of $Te(CN)_4$ and TeF_4. *Angew. Chem. Int. Ed.* **2005**, *44*, 5079-5082.

(20) Fritz, S.; Ehm, C.; Lentz, D. Structure and Chemistry of $SeF_x(CN)_4$-x Compounds. *Inorg. Chem.* **2015**, *54*, 5220-5231.

(21) Tolles, W. M; Gwinn, W. D. Structure and Dipole Moment for SF_4. *J. Chem. Phys* **1962**, *36*, 1119-1121.

(22) Kimura, K.; Bauer, S. H. Electron Diffraction Study of the Molecular Structures of Sulfur Tetrafluoride (SF_4) and Thionyl Tetrafluoride (SOF_4). *J. Chem. Phys* **1963**, *39*, 3172-3178.

(23) Yufit, D. S.; Howard, J. A. K. Cyclopentanone and Cyclobutanone. *Acta Crystallogr., Sect. C* **2011**, *67*, o104-o106.

(24) Jaffe, R. L.; Smith, G. D.; Yoon, D. Y. Conformation of 1,2-Dimethoxyethane from Ab Initio Electronic Structure Calculations. *J. Phys. Chem.* **1993**, *97*, 12745-12751.

(25) Richtera, L.; Toužín, J. Donor-Akceptorové Sloučeniny Oxidu Sírového a 1, 4-Dioxanu. *Chemické listy* **2004**, 633-633.

(26) Christe, K.O.; Curtis, E.C.; Dixon, D.A. On the Problem of Heptacoordination: Vibrational Spectra, Structure, and Fluxionality of Iodine Heptafluoride. *J. Am. Chem. Soc.* **1993**, *115*, 1520-1526.

(27) Christe, K.O.; Wilson, W.W.; Dixon, D.A.; Boatz, J.A. Heptacoordination. Synthesis and Characterization of the IOF_5^{2-} Dianion, and XOF_5E Species *J. Am. Chem. Soc.* **1999**, *121*, 3382-3385.

(28) Christe, K.O.; Curtis, E.C.; Dixon, D.A.; Mercier, H.P.; Sanders, J.C.; Schrobilgen, G.J. Heptacoordination. Synthesis and Characterization of the IOF_5^{2-} Dianion, an XOF_5E Species. *J. Am. Chem. Soc.* **1991**, *113*, 3351-3361.

(29) (a) Mahjoub, A. R.; Seppelt, K. The Structure of IF_6^-. *Angew. Chem. Int. Ed. Engl.* **1991**, *30*, 323-324; (b) Mahjoub, A. R.; Zhang, X.; Seppelt, K. Reactions of the "Naked" Fluoride Ion: Syntheses and Structures of SeF_6^{2-} and BrF_6^- *Chem. Eur. J.* **1995**, *1*, 261-265.

(30) Cadioli, B.; Gallinella, E.; Coulombeau, C.; Jobic, H.; Berthier, G. Geometric Structure and Vibrational Spectrum of Tetrahydrofuran. *J. Phys. Chem.* **1993**, *97*, 7844-7856.

(31) Cataliotti, R.; Paliani, G. Vibrational Spectrum of Crystalline Cyclopentanone *Chem. Phys. Lett.* **1973**, *20*, 280-283.

(32) Yoshida, H.; Matsuura, H. Vibrational Spectrum of Crystalline Cyclopentanone. *J. Phys. Chem. A* **1998**, *102*, 2691-2699.

(33) Christe, K. O.; Zhang, X.; Sheehy, J. A.; Bau, R. Crystal Structure of ClF_4^+ SbF_6^-, Normal Coordinate Analyses of ClF_4^+, BrF_4^+, IF_4^+, SF_4, SeF_4, and TeF_4, and Simple Method for Calculating the Effects of Fluorine Bridging on the Structure and Vibrational Spectra of Ions in a Strongly Interacting Ionic Solid. *J. Am. Chem. Soc.* **2001**, *123*, 6338-6348.

(34) Koch, U.; Popelier, P. L. A. Characterization of C-H-O Hydrogen Bonds on the Basis of the Charge Density. *J. Phys. Chem.* **1995**, *99*, 9747-9754.

(35) Laurence, C.; Gal, J. F. *Lewis Basicity and Affinity Scales*; John Wiley and Sons: Chichester, 2010; Chapter 3.

(36) Gerken, M.; Dixon, D. A.; Schrobilgen, G. J. The OsO_4F^-, $OsO_4F_2^{2-}$, and $OsO_3F_3^-$ Anions, Their Study by Vibrational and NMR Spectroscopy and Density Functional Theory Calculations, and the X-ray Crystal Structures of $[N(CH_3)_4][OsO_4F]$ and $[N(CH_3)_4][OsO_3F_3]$. *Inorg. Chem.* **2000**, *39*, 4244-4255.

(37) *APEX* 2, Version 2.2-0; Bruker AXS Inc.: Madison, WI, **2007**.

(38) Sheldrick, G. M. *SADABS*, Version 2007/4, Bruker ACS Inc.; Madison, WI, **2007**.

(39) Sheldrick, G. M. *SHELXTL2014/6*, University of Göttingen, Germany, **2014**.

(40) Frisch, M. J.; Trucks, G. W.; Schlegel, H. B.; Scuseria, G. E.; Robb, M. A.; Cheeseman, J.R.; Scalmani, G.; Barone, V.; Mennucci, B.; Petersson, G. A.; Nakatsuji, H.; Caricato, M.; Li, X.; Hratchian, H. P.; Izmaylov, A. F.; Bloino, J.; Zheng, G.; Sonnenberg, J. L.; Hada, M.; Ehara, M.; Toyota, K.; Fukuda, R.; Hasegawa, J.; Ishida, M.; Nakajima, T.; Honda, Y.; Kitao, O.; Nakai, H.; Vreven, T.; Montgomery, J. A., Jr.; Peralta, J. E.; Ogliaro, F.; Bearpark, M.; Heyd, J. J.; Brothers, E.; Kudin, K. N.; Staroverov, V. N.; Kobayashi, R.; Normand, J.; Raghavachari, K.; Rendell, A.; Burant, J. C.; Iyengar, S. S.; Tomasi, J.; Cossi, M.; Rega, N.; Millam, N. J.; Klene, M.; Knox, J. E.; Cross, J. B.; Bakken, V.; Adamo, C.; Jaramillo, J.; Gomperts, R.; Stratmann, R. E.; Yazyev, O.; Austin, A. J.; Cammi, R.; Pomelli, C.; Ochterski, J. W.; Martin, R. L.; Morokuma, K.; Zakrzewski, V. G.; Voth, G. A.; Salvador, P.; Dannenberg, J. J.; Dapprich, S.; Daniels, A. D.; Farkas, Ö.; Foresman, J. B.; Ortiz, J. V.; Cioslowski, J.; Fox, D. J. Gaussian 09, Revision D.01; Gaussian, Inc: Wallingford, CT, **2009**.

(41) NBO 6.0. Glendening, E. D.; Badenhoop, J. K.; Reed, A. E.; Carpenter, J. E.; Bohmann, J. A.; Morales, C. M.; Landis, C. R.; Weinhold, F. Theoretical Chemistry Institute, University of Wisconsin, Madison, **2013**.

(42) AIM11 (Version 14.06.21), Todd A. Keith, TK Gristmill Software, Overland Park KS, USA **2014** (aim.tkgristmill.com).

(43) GaussView, version 3.0; Gaussian Inc.: Pittsburgh, PA, 2003.

Table of Contents Graphic and Caption

Sulfur tetrafluoride forms weak Lewis acid-base adducts with organic oxygen-bases, such as ethers and ketones. In these adducts, sulfur accepts chalcogen bonds from two oxygens.